IEICE TRANS. COMMUN., VOL.E94–B, NO.5 MAY 2011

PAPER *Special Section on Antenna and Propagation Technologies Contributing to Diversification of Wireless Technologies*

Transition from Waveguide to Two Microstrip Lines with Slot Radiators in the Millimeter-Wave Band

Kazuyuki SEO[†a)], ***Student Member***, **Kunio SAKAKIBARA**[††], ***Member***, ***and*** **Nobuyoshi KIKUMA**[††], ***Fellow***

SUMMARY Many kinds of microstrip array antennas have been developed in the millimeter-wave band. In order to avoid feeding loss and the decrease of antenna gain by beam shift due to frequency changes, center-fed array antennas are advantageous. In this case, the element spacing around the feeding circuit of the transition from the waveguide to two microstrip lines is larger than one wavelength. Therefore, the sidelobe level grows significantly. In order to suppress the sidelobe level, we propose transitions with slot radiators. Moreover, any polarization angles can be achieved by changing the slot angle. A wide variety from 1.5% to 70% of slot radiator coupling powers can be achieved. To investigate the performance of the proposed transition, 10, 22 and 30-element center-fed microstrip comb-line antennas with the proposed transition were developed at 76.5 GHz, and measured performance was evaluated in the millimeter-wave band.

key words: *microstrip transition, millimeter-wave circuit, waveguide transition, comb-line antenna*

1. Introduction

Many kinds of automotive radars have been developed in the millimeter-wave band [1], [2]. Microstrip antennas are superior candidates when radar sensors are used extensively in vehicles due to their advantages of low cost and low profile. On the other hand, feeding loss due to transmission loss of microstrip lines is a significant problem in array feeding. So, microstrip array antennas are suitable for relatively low gain applications such as the subarrays of digital beam forming (DBF) systems [3]. Series feeding patch array antennas and microstrip comb-line antennas are more effective for relatively low loss compared to ordinary parallel feeding patch array antennas since feeding loss is smaller [4], [5].

Series feeding patch array antennas and microstrip comb-line antennas fundamentally have a significant problem of long line effect [4], causing gain to be degraded by beam shift due to frequency changes when the array antenna is fed from the edge of the microstrip line. So, in some applications, center-fed microstrip array antennas are more advantageous than edge-fed microstrip array antennas [5], as beams do not shift in radiation patterns [6], [7]. Generally, microstrip array antennas are placed on the front surface of radar sensors and are connected to backed millimeter-wave circuits via waveguides in the sensors. Therefore, transitions from waveguides to microstrip lines are required for antenna feeding.

Various types of transitions from waveguide to microstrip line have been proposed. With regard to perpendicular connections, conventional types of probe feeding have wideband characteristics [8], [9], but this requires a metal short block with a quarter-wavelength on the substrate. A replacement for the metal short block is a patch element in the waveguide to achieve sufficient coupling between the waveguide and the microstrip line [10], [11]. The slot coupling type [10] achieves coupling between the microstrip line and the patch element in the waveguide by means of a slot. It is composed of two dielectric substrates without a metal short block. The proximity coupling type has been developed more recently. It can be comprised of a single dielectric

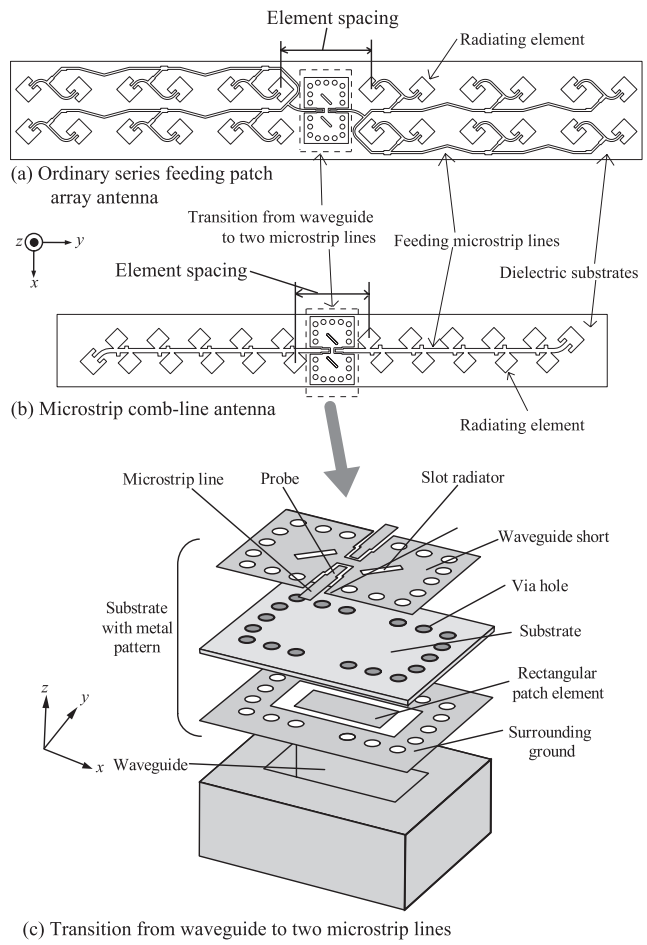

Fig. 1 Configuration of the proposed transition.

Manuscript received August 26, 2010.
Manuscript revised December 17, 2010.

[†]The author is with Nippon Pillar Packing Co., Ltd., Sanda-shi, 669-1333 Japan.
[††]The authors are with Nagoya Institute of Technology, Nagoya-shi, 466-8555 Japan.
a) E-mail: k_seo1951@pure.ocn.ne.jp

DOI: 10.1587/transcom.E94.B.1184

substrate attached to the waveguide end and is suitable for mass production [11].

When a center-fed microstrip array antenna is fed with a previously-developed transition [12], element spacing around the feeding circuit of the transition from the waveguide to the two microstrip lines is larger than one wavelength as shown in Figs. 1(a), (b). Therefore, the sidelobe level grows significantly [7], [13].

In this paper, in order to suppress the sidelobe level, a transition from the waveguide to two microstrip lines with slot radiators is proposed in the millimeter-wave band. This transition can be composed of a single dielectric substrate attached to the waveguide end. The configuration of the transition is presented in Sect. 2. A numerical investigation of the transition shows the relations between the coupling power of the slot radiators and each parameter in Sect. 3. In order to evaluate the performance of the proposed transition, three center-fed microstrip comb-line antennas that use different numbers of elements with the proposed transition are designed as in Sect. 4 and their measured performances are presented in Sect. 5.

2. Configuration

The configuration of the transition is shown in Fig. 1(c). The conductor patterns on both surfaces of the dielectric substrate are separately illustrated in Fig. 1(c). Microstrip lines, probes and waveguide shorts are located on the upper plane of the dielectric substrate. Two slots are patterned symmetrically on the waveguide short. A rectangular patch element and the surrounding ground are patterned on the lower plane of the dielectric substrate. Via holes surround the aperture of the waveguide on the lower plane of the substrate to connect the lower surrounding ground and the upper waveguide short electrically. Input power from the waveguide excites y-component currents on the patch, which couples to the microstrip line probes. The currents on the waveguide short cross the slot radiators, simultaneously. Consequently, radiation is generated from the slot radiators.

The parameters and coordinate systems of the transition are shown in Fig. 2. Parameters are defined as the width W and length L of the rectangular patch element, the broad wall length a and narrow wall length b of the waveguide, the distance S_s between the two slots, the length L_s, width W_s and inclined angle D_s of the slot, the width W_m of the microstrip line, the width W_p of the probe, the width G of the gap between the waveguide short pattern and the microstrip line or the probe, the overlap length ρ of the inserted probe on the rectangular patch element, the thickness T of the dielectric substrate, the relative permittivity ε_r, the diameter ϕ of the via hole, and the spacing S between via hole centers. The parameters of the calculation model are presented in Table 1 for the design frequency range from 76 to 77 GHz. Numerical investigation was carried out using the finite element method.

Mode conversion from the waveguide to the microstrip line is achieved by resonance of the rectangular patch element. The dominant TE_{10} mode of the waveguide is converted to the quasi-TEM mode of the microstrip line. Figure 3 shows the calculated electric field intensity distribution in the xy-plane including the CC'-line. The electric field intensity E includes all the x, y and z components of the electric field. We observed that the electric field intensities of both sides of the slot radiators were large enough to generate radiation.

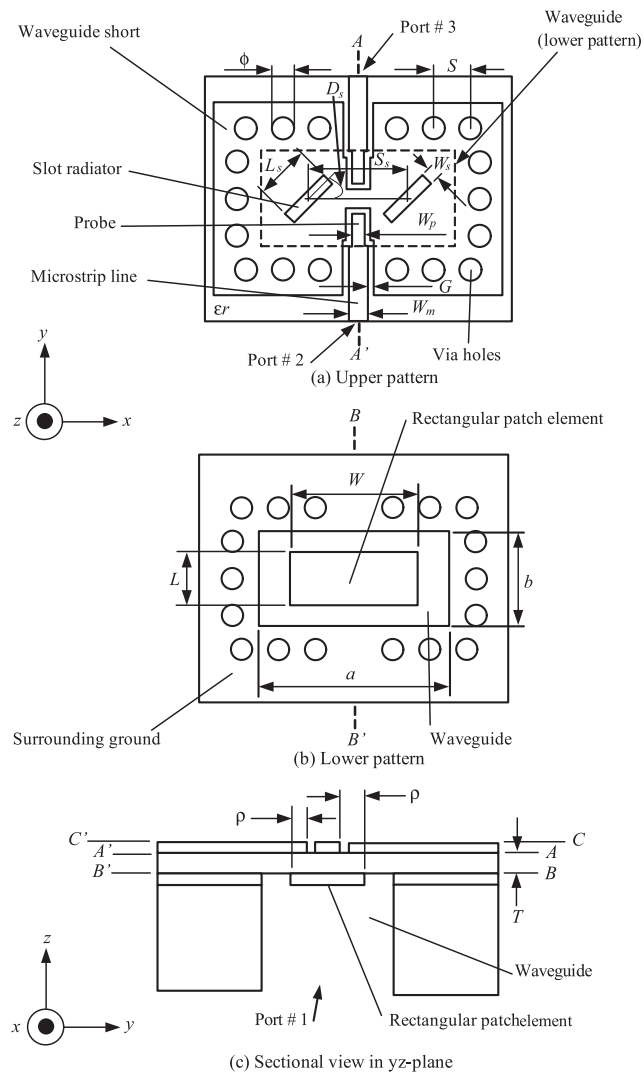

Fig. 2 Parameters and coordinate systems.

Fig. 3 Electric field intensity distribution in the xy-plane including the CC'-line.

3. Numerical Investigation

To verify the relationships between the coupling power of the slot radiators and each parameter, the transition illustrated in Fig. 2 was investigated numerically by using an electromagnetic simulator based on the finite-element method. The dimensions of the waveguide are those of the WR-12 standard waveguide. The width of the microstrip line W_m is 0.3 mm, corresponding to approximately 52 Ω of characteristic impedance. In this calculation, the loss tangent $\tan\delta = 0.001$ is used as a loss factor of dielectric loss. Regarding conductivity, it has been reported that the conductivity of the inner surface of a copper-clad is decreased to 18% compared to the bulk copper conductivity in microwave band [14]. In this case, surface conductivity could be decreased to $\sigma = 1.0 \times 10^7$ S/m. However, decrease of the conductivity depends on the manufacture of the copper-clad laminated substrate. So, in this calculation, conductivity $\sigma = 5.8 \times 10^7$ S/m is used as a loss factor. In order to estimate the coupling power of the slot radiators, the effect to decrease conductivity is studied in Sect. 3.2.

3.1 Scattering Parameters

The reflection characteristics of the transition with the parameters in Table 1 are presented in Fig. 4. The simulation results show that the bandwidth for $|S_{11}|$ below −15 dB is 3.1 GHz, and the transmission characteristics $|S_{21}|$ and $|S_{31}|$ are from −4.21 dB to −4.45 dB in the frequency range from 76 GHz to 77 GHz, where the loss-less transmission characteristics $|S_{21}|$ and $|S_{31}|$ of the transition without the slot radiators are 0.5 or −3 dB for equal power divider.

The length L of the rectangular patch element affects the resonant frequency as shown in Fig. 4. Increasing the length L of the rectangular patch element causes lower resonant frequency. So, the operating frequency of this transition can be controlled by the length L of the rectangular patch element.

Table 1 Parameters of calculation model.

Description	Name	Value
Width of patch element	W	2.07 mm
Length of patch element	L	0.725 mm
Broad wall length of waveguide	a	3.1 mm
Narrow wall length of waveguide	b	1.55 mm
Distance between two slots	S_s	1.6 mm
Length of slot	L_s	1.1 mm
Width of slot	W_s	0.2 mm
Inclined angle of slot	D_s	45 deg.
Width of microstrip line	W_m	0.3 mm
Width of probe	W_p	0.2 mm
Width of gap	G	0.1 mm
Overlap length of inserted probe	ρ	0.15 mm
Thickness of substrate	T	0.115 mm
Relative permittivity	ε_r	2.23
Diameter of via hole	ϕ	0.35 mm
Space between via holes	S	0.6 mm

The overlap length ρ of the inserted probe on the rectangular patch element affects the coupling or the impedance as shown in Fig. 5. Increasing the overlap length ρ increases the capacitive reactance at the desired frequency, and decreasing the overlap length ρ increases the inductive reactance. Furthermore, the width W_p of the probe affects the impedance as well shown in Fig. 6. Increasing the width W_p of the probe increases the capacitive reactance at the desired frequency, and decreasing the width W_p of the probe increases the inductive reactance. So, impedance matching can be controlled by adjusting the overlap length ρ of the inserted probe and the width W_p of the probe in order to cancel reactive components.

3.2 Coupling Power of Slot Radiators

The coupling power from the slots to the air is evaluated accurately including the effect of the perturbed current distribution around the slots as following procedure.

The coupling powers of the slot radiators were calculated for each design from scattering parameters, which were obtained by an electromagnetic simulation.

A sum of the coupling powers of the slot radiators and the total loss of the proposed transition were calculated, that is,

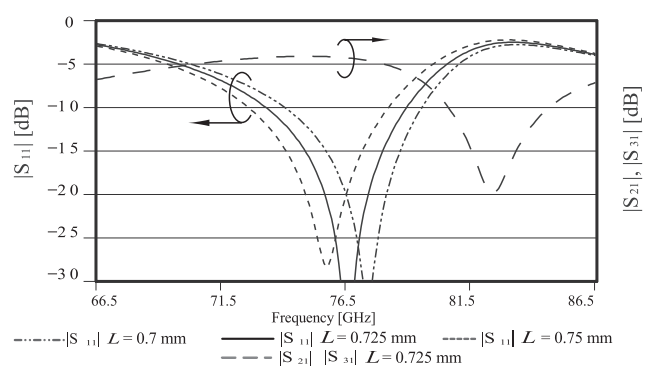

Fig. 4 $|S_{11}|$ according to length of the rectangular patch element L and transition characteristics $|S_{21}|$ and $|S_{31}|$.

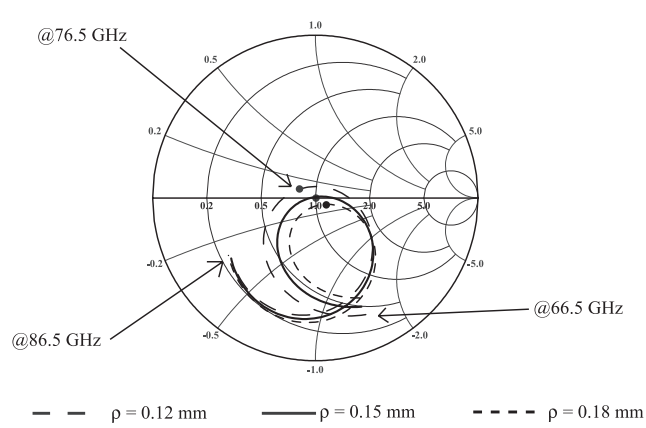

Fig. 5 Relation between impedance and overlap length ρ of the inserted probe from 66.5 GHz to 86.5 GHz.

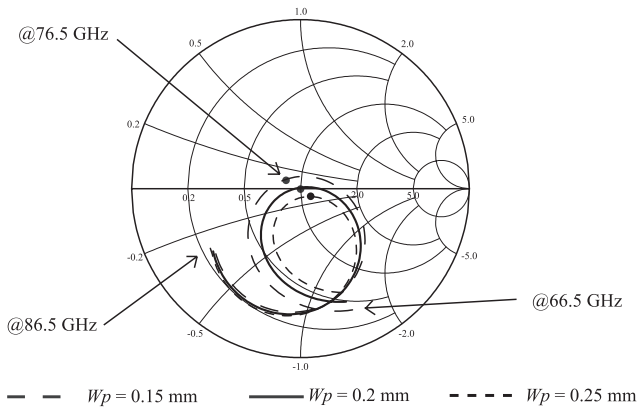

Fig. 6 Relation between impedance and width W_p of the probe from 66.5 GHz to 86.5 GHz.

$$L1 = 1 - |S_{11}|^2 - |S_{21}|^2 - |S_{31}|^2 \quad [\times 100\%] \tag{1}$$

where $|S_{11}|$, $|S_{21}|$ and $|S_{31}|$ are simulated scattering parameters of the transmission. This total loss include dielectric loss of the substrate and conductor loss.

In order to calculate the coupling powers of the slot radiators, the total loss must be evaluated. For the conductor loss, strong currents flow around the slot radiators of the waveguide short. Therefore, the conductor loss depending on conductivity of the waveguide short was evaluated, that is,

$$L2 = 1 - |S_{11}'|^2 - |S_{21}'|^2 - |S_{31}'|^2 \quad [\times 100\%] \tag{2}$$

where S_{11}', S_{21}' and S_{31}' are simulated scattering parameters of the transmission when the waveguide short is assumed to be a perfect electric conductor. Equation (2) indicates a sum of the coupling powers of the slot radiators and the total loss of the transition when the waveguide short is assumed to be a perfect electric conductor. This loss does not include conductor loss of the waveguide short unlike the Eq. (1).

The conductor loss of the waveguide short was calculated as,

$$L3 = L1 - L2 \quad [\times 100\%] \tag{3}$$

Equation (3) shows the conductor loss of the waveguide short caused by strong currents around the slot radiators.

In order to evaluate dielectric loss of the substrate and conductor loss excluding conductor loss of the waveguide short, the loss $L4$ is evaluated as,

$$L4 = 1 - |S_{11}''|^2 - |S_{21}''|^2 - |S_{31}''|^2 \quad [\times 100\%] \tag{4}$$

where S_{11}'', S_{21}'' and S_{31}'' are simulated scattering parameters of the transmission without slot radiators and with the waveguide short assumed to be a perfect electric conductor.

The coupling powers of the slot radiators were calculated as,

$$Cs = L1 - L3 - L4 \quad [\times 100\%] \tag{5}$$

In this calculation, radiation form the slot radiators in Eq. (1) is assumed to be the same as in Eq. (2).

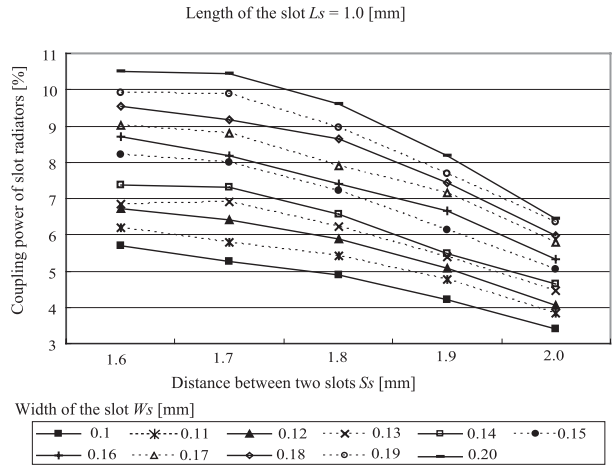

Fig. 7 Coupling powers of slot radiators according to the distance between two slots S_s and the width of the slot W_s when the length of the slot L_s = 1.0 mm.

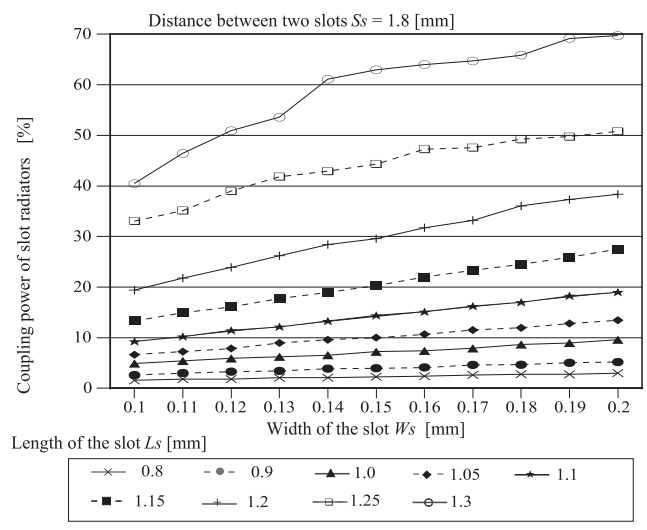

Fig. 8 Coupling power of slot radiators according to slot length L_s and width W_s when the distance between the two slots S_s = 1.8mm.

Relations between the coupling power of the slot radiators and the distance S_s between two slots at each width W_s of the slot when the length L_s of the slot is 1.0 mm were calculated as shown in Fig. 7. The simulation results show that increasing the distance S_s between the two slots decreases the coupling power of the slot radiators. This tendency is the same with other slot length L_s. This is caused by the current intensity distribution on the waveguide short. High current intensity is at the center of the waveguide short, however at the side of the waveguide short, current intensity is low. Figure 8 shows the relation between the coupling power of the slot radiators and the width W_s of the slot at each length L_s of the slot when the distance S_s between the two slots is 1.8 mm. Increasing the width W_s of the slot increases the coupling power of the slot radiators. Increasing the length L_s of the slot also increases the coupling power of the slot radi-

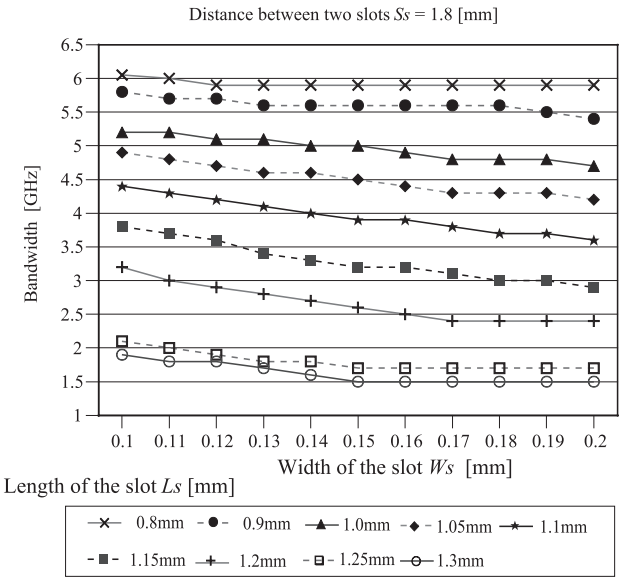

Fig. 9 Bandwidth according to slot length L_s and width W_s when the distance between the two slots S_s = 1.8 mm.

ators. This tendency is the same with the other distances S_s between the two slots. The length L_s of the slot affects most significantly effect on the coupling power of the slot radiators because, a slot with long length L_s cuts many currents. In each calculation, the rectangular patch element length L, the inserted probe overlap length ρ and the probe width W_p are optimized to achieve the lowest reflection characteristics $|S_{11}|$.

When the distance S_s between two slots is small, such as 1.6 mm, the long length L_s of the slot cannot be arranged on the transition because, the long length L_s of the slot causes contact the microstrip line. However, if the distance S_s between two slots is large, it is possible to design with the long length L_s of the slot. The simulation results show that the coupling power of the slot radiators is controlled by the distance S_s between the two slots, the length L_s of the slot and the width W_s of the slot from 1.5% to 70%.

On the other hand, increasing the slot length L_s and the width W_s, which increases the coupling power of the slot radiators, decreases the bandwidth for $|S_{11}|$ below −15 dB as shown in Fig. 9. The coupling power of the slot radiators and the bandwidth of the transition have a trade-off relationship.

When the reduced conductivity is applied as $\sigma = 1.0 \times 10^7$ S/m, the calculated coupling power of the slot radiators increases approximately 1.7% compared with $\sigma = 5.8 \times 10^7$ S/m. So, the calculated coupling power of the slot radiators has an error of less than 1.7%.

4. Design of a Center-Fed Microstrip Comb-Line Antenna with the Proposed Transition

A microstrip comb-line antenna is proposed and applied in this design [5], [15]. The designed center-fed microstrip comb-line antenna is shown in Fig. 10. The antenna is fed by the proposed transition at the center of the microstrip line. In order to suppress reflections from every rectangular radiating element, reflection-canceling stub structures are applied to the feeding microstrip line. These function works in the same way as reflection-canceling slit [15].

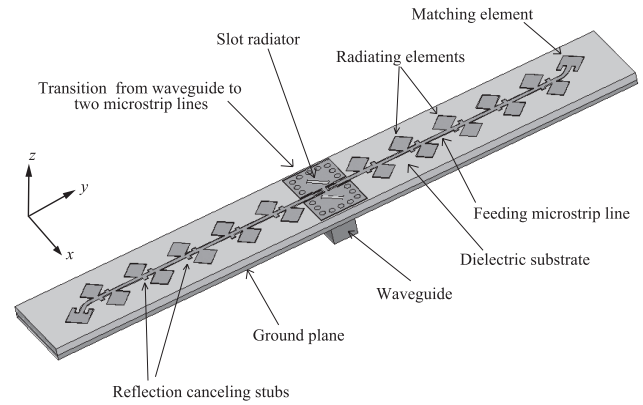

Fig. 10 Configuration of center-fed microstrip comb-line antenna.

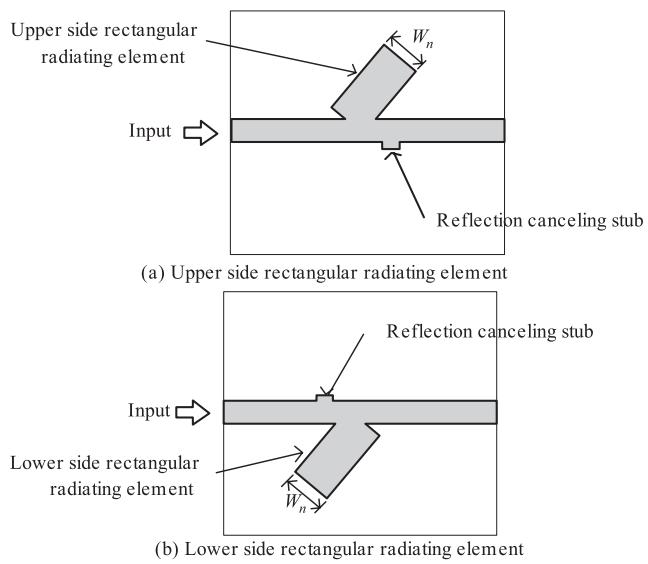

Fig. 11 Structure for electromagnetic analysis of comb-line antenna.

Figure 11 shows the analysis model of the radiating element of the microstrip comb-line antenna. The coupling power from the rectangular radiating element is calculated for each element width W_n with resonant length from scattering parameters $|S_{11}|$ and $|S_{21}|$ obtained by electromagnetic simulation, that is,

$$C_r = 1 - |S_{11}|^2 - \left(\frac{|S_{21}|}{|S_{21}'|}\right)^2 \quad [\times 100\%] \tag{6}$$

where S_{21} shows transmission of the comb-line antenna, which were reduced due to the coupling power of the rectangular radiating element and dielectric loss of the substrate and conductor loss. S_{21}' shows transmission of the microstrip line without a radiating element, which were reduced due to dielectric loss of the substrate and conductor loss. Therefore, reduced power due to the radiating element

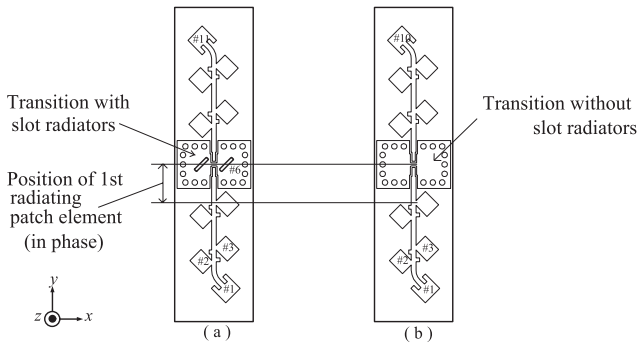

Fig. 12 Overview of 10-element center-fed microstrip comb-line antennas using transitions with and without slot radiators.

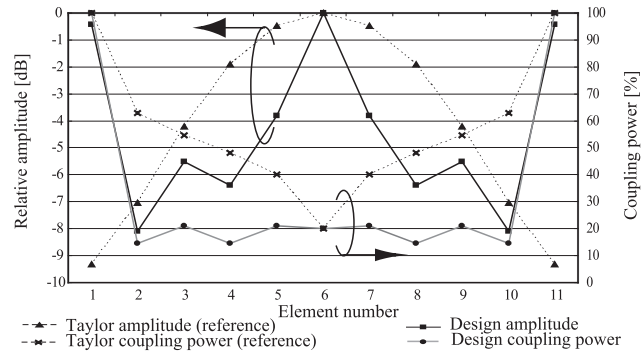

Fig. 13 Aperture amplitude distribution and coupling power for 11-element antenna.

is expressed by $(|S_{21}|/|S_{21}'|)^2$. Scattering parameters of the upper side elements in Fig. 11(a) are different from the lower side elements in Fig. 11(b). Therefore, the coupling power of the rectangular radiating element is evaluated independently.

From the calculations, the coupling power of the rectangular radiating elements can be controlled from 2% up to 20.9% for the upper side elements and from 2% up to 14.6% for the lower side elements shown in Fig. 11 by adjusting the width W_n of the elements from 0.1 mm up to 1.05 mm.

The positions of the two first rectangular radiating elements at the both sides of the transition shown in Fig. 12 are determined to excite in phase with the slot radiators. The spacing between the first radiating elements and the slot radiators are optimized to be the same phase of the simulated electric field just on the radiating element and the center of the two slot radiators.

In array design, the target is a −30 dB Taylor distribution with $\bar{n} = 2$. However, this is difficult to achieve with 10, 22 and 30-elemnt center-fed microstrip comb-line antennas due to the limited coupling power of the rectangular radiating elements. Therefore, possible sidelobe reduction using the proposed transition is investigated by some designs of these element numbers. Three center-fed microstrip comb-line antennas were designed with three different numbers of elements. The basic parameters of the transitions are in Table 1, but the design parameters of the transitions at each design were optimized and changed from Table 1.

4.1 10-Element Center-Fed Microstrip Comb-Line Antenna

To investigate the performance of the proposed transition, 10-element center fed microstrip comb-line antennas were designed using the proposed transition with slot radiators (shown in Fig. 12(a)) and using an ordinary transition without slot radiators (shown in Fig. 12(b)). The target −30 dB Taylor distribution with $\bar{n} = 2$ and coupling power for an 11-element array antenna including slot radiators are shown in Fig. 13 for reference.

In the design of the comb-line antenna, the designed coupling power and amplitude distribution changed as shown in Fig. 13 due to the limited coupling power of the rectangular radiating elements. Consequently, the assigned coupling power of the center radiating element, which is a pair of slot radiators on the proposed transition, was determined to be 19.9%. As a result, the designed amplitude distribution is very different from the target Taylor distribution. To compare comb-line antennas with and without slot radiators, two comb-line antennas were designed. The configuration of the transition for this design, is shown in Fig. 2 and the design parameters are the same as shown in Table 1. Characteristics of this transition are shown in Fig. 4. Figure 14 shows the simulated radiation patterns and array factors in the *yz*-plane at 76.5 GHz.

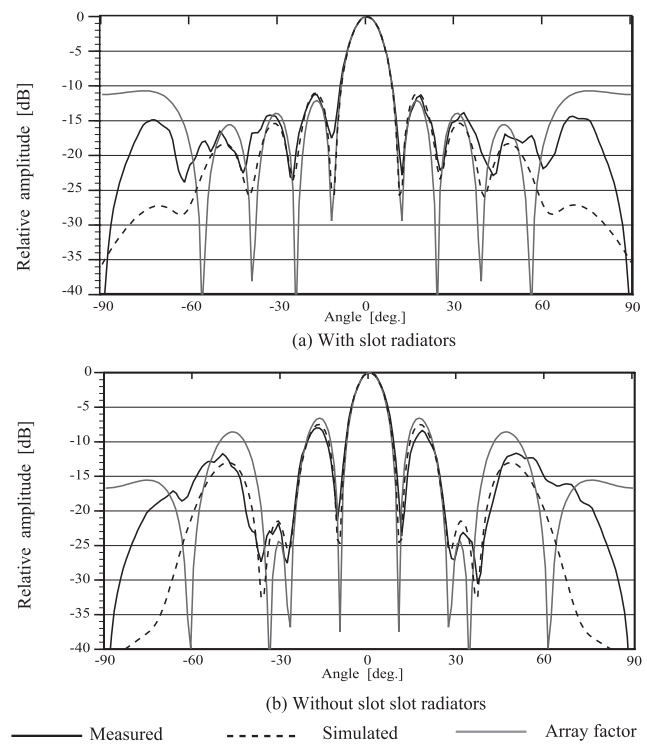

Fig. 14 Radiation patterns in the *yz*-plane of 10-element center-fed microstrip comb-line antennas at a frequency of 76.5 GHz.

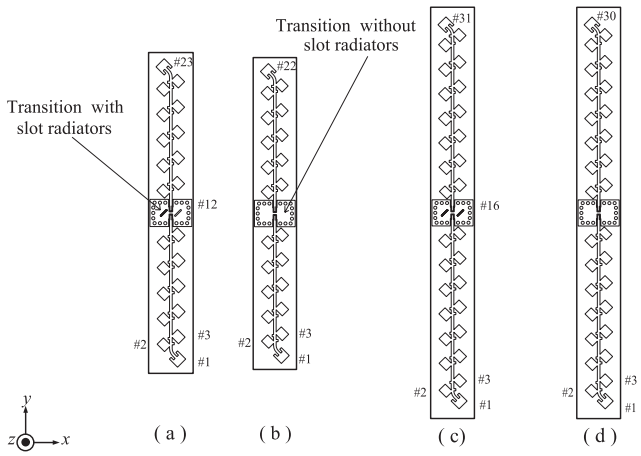

Fig. 15 Overview of 22 and 30-element center-fed microstrip comb-line antennas using transitions with and without slot radiators.

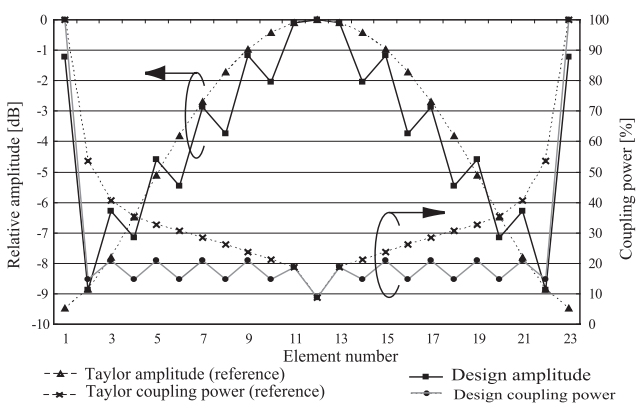

Fig. 16 Aperture amplitude distribution and coupling power for 23-element antenna.

4.2 22 and 30-Element Center-Fed Microstrip Comb-Line Antennas

22-element center fed microstrip comb-line antennas were designed using the proposed transition with slot radiators (shown in Fig. 15(a)) and using an ordinary transition without slot radiators (shown in Fig. 15(b)). In the design of the comb-line antennas, the design coupling powers and amplitude distributions change as shown in Fig. 16 due to the limited coupling power of the rectangular radiating elements. The assigned coupling power of the center radiating element, which is a pair of slot radiators on the proposed transition, was determined to be 8.2%. The configuration of the transition for this design, is shown in Fig. 2. Some parameters must be changed as in Table 2, but other parameters are the same as in Table 1. Figure 17 shows the simulated radiation patterns and array factors in the *yz*-plane at 76.5 GHz.

30-element center-fed microstrip comb-line antennas were designed using the proposed transition with slot radiators (shown in Fig. 15(c)) and using an ordinary transition without slot radiators (shown in Fig. 15(d)). In the design of comb-line antenna, the design coupling powers and amplitude distributions change as shown in Fig. 18 due to the limited coupling power of the rectangular radiating elements. Owing to the increase in the number of radiating elements, required coupling power is decreased. Therefore, design amplitude distribution gets closer to the target Taylor distribution. The assigned coupling power of the center radiating element, which is a pair of slot radiators on the proposed transition, was determined to be 7.2%. The configuration of the transition for this design, is shown in Fig. 2. Some parameters must be changed as in Table 3, but other parameters are the same as in Table 1. Figure 19 shows the simulated radiation patterns and array factors in the *yz*-plane at 76.5 GHz.

Table 2 Parameters of the transition with 8.2% slot radiator coupling power.

Description	Name	Value
Length of patch element	L	0.84 mm
Length of slot	L_s	1.0 mm
Width of slot	W_s	0.15 mm
Overlap length of inserted probe	ρ	0.19 mm

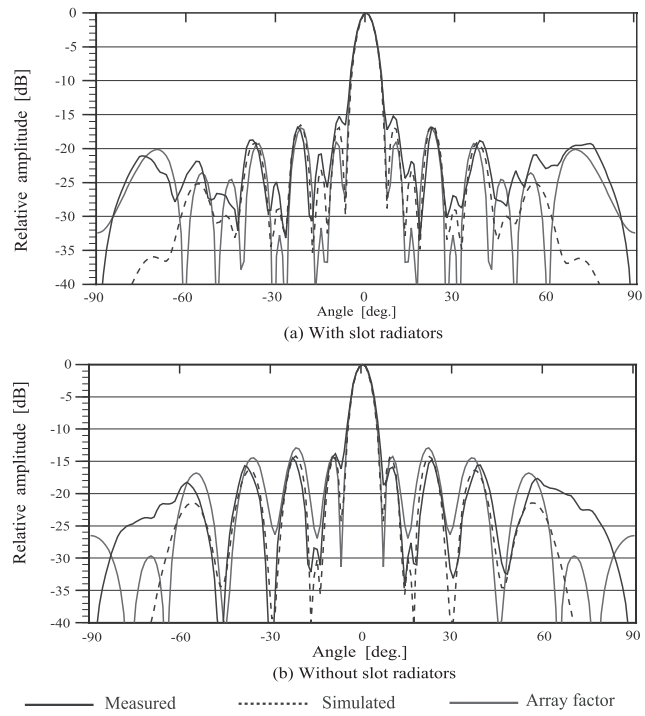

Fig. 17 Radiation patterns in the *yz*-plane of 22-element center-fed microstrip comb-line antennas at a frequency of 76.5 GHz.

Table 3 Parameters of the transition with 7.2% slot radiator coupling power.

Description	Name	Value
Length of patch element	L	0.87 mm
Distance between two slots	S_s	1.8 mm
Length of slot	L_s	1.0 mm
Width of slot	W_s	0.15 mm
Overlap length of inserted probe	ρ	0.2 mm

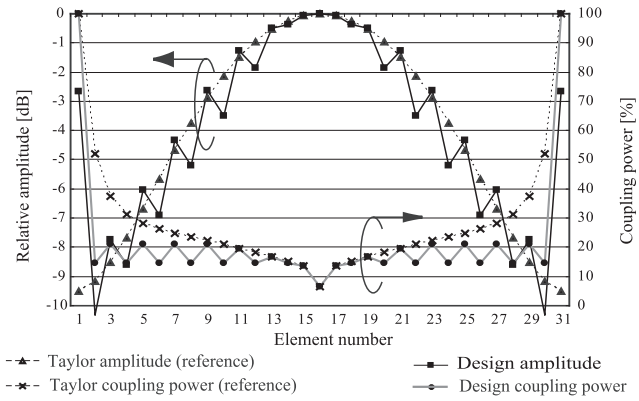

Fig. 18 Aperture amplitude distribution and coupling power for 31-element antenna.

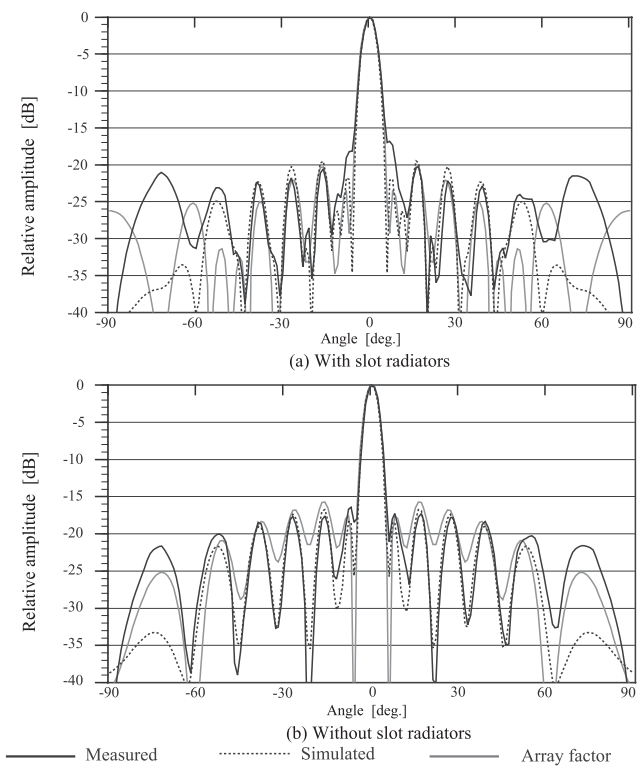

Fig. 19 Radiation patterns in the *yz*-plane of 30-element center-fed microstrip comb-line antennas at a frequency of 76.5 GHz.

5. Experiments

Three length of center-fed microstrip comb-line antennas using the transitions with and without slot radiators in Sect. 4 were fabricated. Figure 20 shows photographs of the developed transition that was designed in Sect. 4.1.

Figure 21 shows characteristics of the transition with a coupling power of 19.9%. In this measurement, the device-under-test (DUT) was comprised of a pair of waveguides connected separately to one microstrip line transition. Microstrip lines were connected at both ends of the transition. At the opposite sides of the microstrip line, a one-waveguide

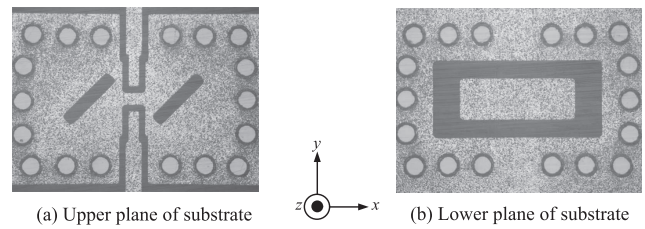

Fig. 20 Fabricated transition.

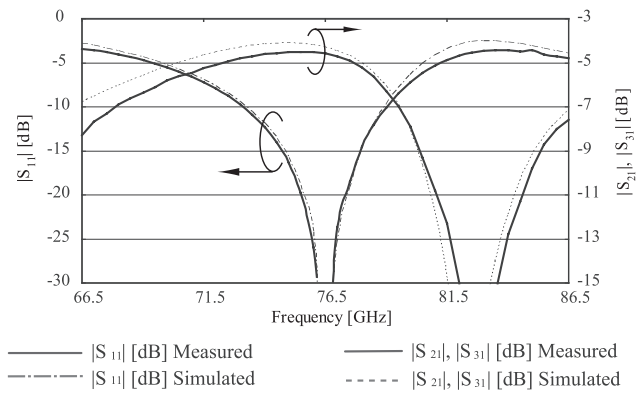

Fig. 21 Characteristics of the transition with 19.9% slot radiator coupling power.

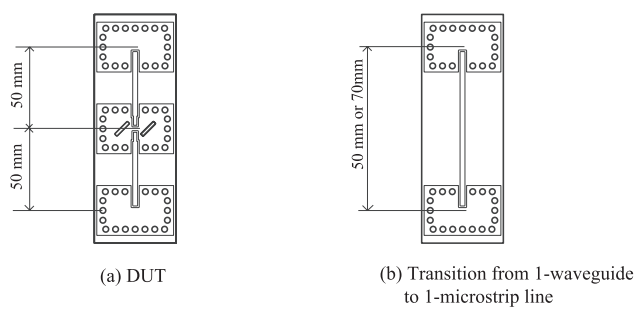

Fig. 22 DUT used for measurement.

to one-microstrip line transition is connected as shown in Fig. 22(a). To measure the loss of a one-waveguide to one-microstrip line transition, a pair of transitions with one microstrip line was composed as shown in Fig. 22(b). The measured $|S_{11}|$, $|S_{21}|$ and $|S_{31}|$ in Fig. 21 were obtained by taking the transmission coefficient of the DUT, subtracting the loss of the microstrip line and the loss of the transition from one-waveguide to one-microstrip line. The loss of the microstrip line was measured as 0.04 dB/mm from 76 to 77 GHz. The loss of the transition from the one-waveguide to one-microstrip line was measured as 0.5 dB from 76 to 77 GHz. A time gate function was used to exclude undesired waves, and high accuracy was achieved in this measurement. The distance between the centers of the waveguides was set at 50 mm or 70 mm, which was long enough to distinguish between desired and undesired waves in the time domain. In this case, the bandwidth for $|S_{11}|$ below −15 dB is 3.12 GHz and the transmission characteris-

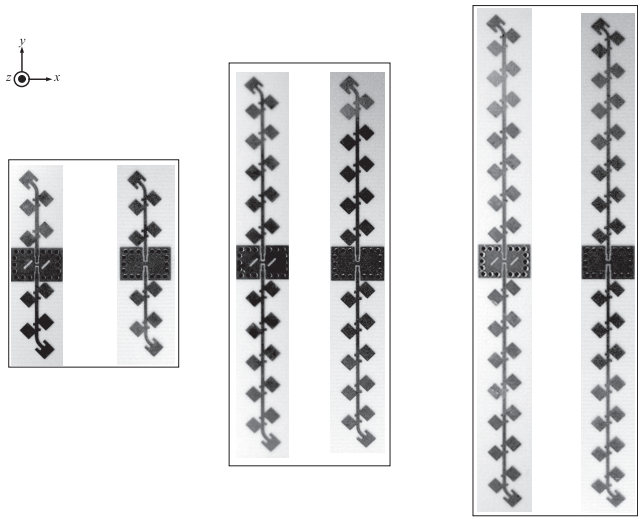

Fig. 23 Fabricated antenna.

tics $|S_{21}|$ and $|S_{31}|$ are from −4.52 dB to −4.75 dB over the frequency range from 76 GHz to 77 GHz. Photographs of the microstrip comb-line antennas developed for each design are shown in Fig. 23.

The measured radiation patterns of the 10, 22 and 30-element comb-line antennas are shown in Figs. 14, 17 and 19, respectively. The first sidelobe angle of each comb-line antenna with slot radiators agrees with the corresponding comb-line antenna without slot radiators in the measured, simulated and array factor results. The measured radiation pattern of each comb-line antenna almost agrees with the simulated results and the array factor in the range from −50 deg. to 50 deg. However, increased sidelobe levels are measured in wide beam angles compared to the simulated results. These far field radiation patterns are obtained by Fourier transformation of the measured near field distributions. Therefore, accuracy is insufficient in wide angles.

For the 10-element antennas, the first sidelobe level of the comb-line antenna with slot radiators decreased by 3.24 dB in measurement, 3.51 dB in simulation and 5.53 dB in array factor compared to the comb-line antenna without slot radiators.

For the 22-element antennas, the first sidelobe level of the comb-line antenna with slot radiators decreased by 1.25 dB in measurement, 2.52 dB in simulation and 4.72 dB in array factor compared to the comb-line antenna without slot radiators.

For the 30-element antennas, the first sidelobe level of the comb-line antenna with slot radiators decreased by from 0.5 dB to 1.77 dB in measurement, 3.42 dB in simulation and 5.92 dB in array factor compared to the comb-line antenna without slot radiators.

6. Conclusion

We developed a transition from waveguide to two microstrip lines with slot radiators in the millimeter-wave band. A coupling power of the slot radiators from 1.5% to 70% was achieved by using an electromagnetic simulator. Three center-fed comb-line antennas with the proposed transitions and different numbers of elements (10, 22 and 30) were designed and fabricated, resulting in 19.9%, 8.2% and 7.2% slot radiator coupling power at 76.5 GHz. The measured first sidelobe level of each designed array antenna decreased by 0.5 dB to 3.24 dB. In each design, it was confirmed that the coupling power of the slot radiators on the proposed transition could be controlled and was useful to suppress the sidelobe level sufficiently.

References

[1] M.E. Russel, C.A. Drubin, A.S. Marinilli, and W.G. Woodington, "Integrated automotive sensors," IEEE Trans. Microw. Theory Tech., vol.50, no.3, pp.674–677, March 2002.

[2] S. Tokoro, K. Kuroda, and A. Kawakubo, "Automotive electronically scanned millimeter-wave radar," SICE Annual Conference, vol.1, pp.42–47, Aug. 2003.

[3] A. Asano, "Millimeter-wave holographic radar for automotive applications," 2000 Microwave Workshops and Exhibition Digest, MWE 2000, pp.157–162, Dec. 2000.

[4] J.R. James and P.H. Hall, Handbook of microstrip antennas, IEEE Electromagnetic Waves Series, vol.2, Peter Peregrinus Ltd., London, UK, 1989.

[5] H. Iizuka, T. Watanabe, K. Sato, and K. Nishikawa, "Millimeter-wave microstrip array antenna for automotive radar," IEICE Trans. Commun., vol.E86-B, no.9, pp.2728–2738, Sept. 2003.

[6] Y. Ikeno, K. Sakakibara, N. Kikuma, and H. Hirayama, "Narrow-wall-slotted hollow-waveguide array antenna using partially parallel feeding system in millimeter-wave band," IEICE Trans. Commun., vol.E93-B, no.10, pp.2545–2553, Oct. 2010.

[7] A. Kunita, K. Sakakibara, N. Kikuma, and H. Hirayama, "Measured performance of center-fed microstrip comb-line antenna in millimeter-wave," Proc. Commun. Conf. IEICE 2009, B-1-158, p.158, Sept. 2009.

[8] T.Q. Ho and Y.C. Shih, "Spectral-domain analysis of E-Plane waveguide to microstrip transitions," IEEE Trans. Microw. Theory Tech., vol.37, no.2, pp.388–392, Feb. 1989.

[9] Y. Leong and S. Weinreb, "Full band waveguide to microstrip probe transitions," IEEE MTT-S Int. Microw. Symp. Dig., vol.4, pp.1435–1438, Anaheim, CA, May 1999.

[10] W. Grabherr, B. Hudder, and W. Menzel, "Microstrip to waveguide transition compatible with mm-wave integrated circuits," IEEE Trans. Microw. Theory Tech., vol.42, no.9, pp.1842–1843, Sept. 1994.

[11] H. Iizuka, T. Watanabe, K. Sato, and K. Nishikawa, "Millimeter-wave microstrip line to waveguide transition fabricated on a single layer dielectric substrate," IEICE Trans. Commun., vol.E85-B, no.6, pp.1169–1177, June 2002.

[12] D. Wu and K. Seo, "Waveguide to microstrip line transition and power divider," Electron. Lett., vol.43, no.3, pp.169–170, Feb. 2007.

[13] K. Hashimoto, J. Hirokawa, and M. Ando, "Parallel plate slot array fed by post-wall center-feed waveguide consisting of T-junctions," IEEE Antennas and Propagation Society International Symposium, 2008 AP-S, pp.1–4, 2008.

[14] Y. Kobayashi, "Microwave evaluation techniques of copper-clad dielectric laminated substrates," IEICE Trans. Electron. (Japanese Edition), vol.J89-C, no.5, pp.210–216, May 2006.

[15] Y. Kashino, K. Sakakibara, Y. Hayashi, N. Kikuma, and H. Hirayama, "Design of millimeter-wave microstrip comb-line antenna array beam-tilting in perpendicular plane of feeding line," IEICE Trans. Commun. (Japanese Edition), vol.J90-B, no.9, pp.864–872, Sept. 2007.

Kazuyuki Seo was born in Okayama, Japan, on July 5, 1951. He received a B.S. degree in Electrical Engineering from Okayama University, in 1975. From 1985 to 2001, he worked at Kojima Press Industry Co., Ltd., in Aichi, and was engaged in the development of antennas for mobile communication systems. He has 21 years of industrial experience in automotive antennas. He is presently a Ph.D. student at the School of Computer Science and Engineering, Nagoya Institute of Technology. His research interests are antennas for mobile communication systems and radar systems.

Kunio Sakakibara was born in Aichi, Japan, on November 8, 1968. He received the B.S. degree in Electrical and Computer Engineering from Nagoya Institute of Technology, Nagoya, Japan, in 1991, the M.S. and D.E. degrees in Electrical and Electronic Engineering from Tokyo Institute of Technology, Tokyo, Japan in 1993 and 1996, respectively. From 1996 to 2002, he worked at Toyota Central Research and Development Laboratories, Inc., Aichi, and was engaged in the development of antennas for millimeter-wave automotive radar systems. From 2000 to 2001, he was with the department of Microwave Techniques in the University of Ulm, Ulm, Germany, as a Guest Researcher. He was a lecturer at Nagoya Institute of Technology from 2002 to 2004, and is currently an Associate Professor. His research interest is in millimeter-wave antennas and circuits. Dr. Sakakibara is a senior member of IEEE.

Nobuyoshi Kikuma was born in Ishikawa, Japan, on January 7, 1960. He received the B.S. degree in electronic engineering from Nagoya Institute of Technology, Japan, in 1982, and the M.S. and Ph.D. degrees in electrical engineering from Kyoto University, Japan, in 1984 and 1987, respectively. From 1987 to 1988, he was a Research Associate at Kyoto University. In 1988 he joined Nagoya Institute of Technology, where he has been a Professor since 2001. His research interests include adaptive and signal processing array, multipath propagation analysis, mobile and indoor wireless communication, and electromagnetic field theory. He received the 4th Telecommunications Advancement Foundation Award in 1989. Dr. Kikuma is a senior member of the IEEE.